Impact of Cross-Polarization Interference on Dual Polarization Communication Systems

Edgar Satorius*, Thomas Jedrey†, and Charles Wang*

ABSTRACT. — In this article we present an analysis of the impact of cross-polarization interference on the performance of wideband dual polarization communication systems with particular emphasis on the Surface Water and Ocean Topography (SWOT) X-band satellite communication system. SWOT transmits dual-polarized (right and left hand circular polarizations), offset-QPSK (OQPSK) modulated signals with a 310-Mbps information rate per polarization channel using the Earth Exploration Satellite Service (EESS) band: 8025–8400 Megahertz (MHz). Cross-polarization interference arises in several different ways including: (i) conversion of cross-polarization (cross-pol) to co-polarization (co-pol) interference due to reflections off the spacecraft structure (termed multipath); (ii) conversion of cross-pol to co-pol interference due to the cross-pol gains of the transmitting and receiving antennas and (iii) tropospheric depolarization. The ratio of co-pol power to the cross-pol converted "leakage" power is defined as cross-pol discrimination (XPD). The analysis presented in this article derives bit error rate (BER) formulas as a function of the number of reflected paths; the delay and XPD of each path, and the received signal-to-noise ratio. Furthermore, simple approximate BER formulas are derived that can be used to bound system performance based on parameter estimates obtained from an antenna model developed to predict SWOT performance.

I. Introduction

In designing a dual polarization communications system, interference from cross-polarized signals is a critical concern. Such interference can arise in several different ways including: (i) conversion of cross-polarization (cross-pol) to co-polarization (co-pol) interference due to reflections off the spacecraft structure (termed multipath); (ii) conversion of cross-pol to co-pol interference due to the cross-pol gains of the transmitting and receiving antennas; and (iii) tropospheric depolarization [1]. The ratio of co-pol power to the cross-pol converted "leakage" power is defined as cross-pol discrimination (XPD). This occurs for both polarization channels. Furthermore, weather can also turn a portion

*Flight Communications System Section

†Communications, Tracking, and Radar Division

The research described in this publication was carried out by the Jet Propulsion Laboratory, California Institute of Technology, under a contract with the National Aeronautics and Space Administration.

of the cross-pol signal into the co-pol signal thereby interfering with the co-pol link and vice versa.

In this article, we consider these effects with particular emphasis on the Surface Water and Ocean Topography (SWOT) X-band communication system. SWOT transmits dual-polarized (right and left hand circular polarizations, RHCP and LHCP), offset quadrature phase-shift keying (OQPSK) modulated signals with a 310 megabits per second (Mbps) information rate per polarization channel using the Earth Exploration Satellite Service (EESS) band: 8025–8400 megahertz (MHz). Centre National d'Etudes Spatiales (CNES) 11-m/13-m ground stations will receive the transmissions, which employ Reed-Solomon (255,223) coding resulting in a coded OQPSK symbol rate of 177.8 megasymbols per second (Msps) per polarization channel. A SWOT system diagram is shown in Figure 1.

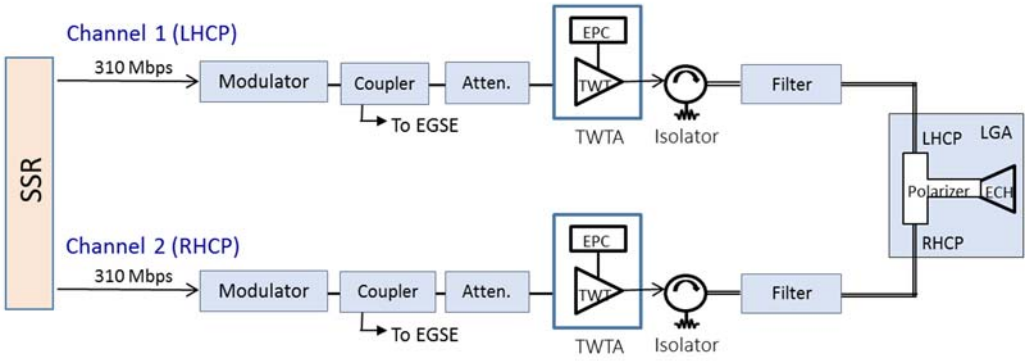

Figure 1. SWOT X-band telecom block diagram.

The RHCP and LHCP outputs from the solid-state recorder (SSR) are modulated, attenuated, and fed into the traveling-wave tube amplifier (TWTA) assembly. The TWTA comprises the traveling-wave tube (TWT) and the electronic power conditioner (EPC). The modulator outputs are also routed into electronic ground support equipment (EGSE) via couplers. The outputs from the TWTAs are then filtered and combined in the low-gain antenna (LGA) assembly. The LGA is based on an externally corrugated horn (ECH) design.

In the remainder of this article, we will first consider in Section II the impact of a single OQPSK cross-pol interferer on an OQPSK (co-pol) communications system. To evaluate the degradation, analyses and simulations have been performed. The cross-pol interference is modeled as an uncorrelated OQPSK signal scaled by the reciprocal of XPD and rotated by a phase. Simulation results of uncoded OQPSK links and Reed-Solomon (255,223)-coded OQPSK links are presented. We then extend this analysis in Section III to the general case wherein the interference is modeled as a superposition of delayed versions of an uncorrelated OQPSK signal, which represents the opposite (or cross-pol) transmission, scaled by the reciprocal of XPD and rotated by a phase. The delayed cross-pol interference components, which represent reflections off the surrounding spacecraft structures, create an interference multipath condition. It should be noted that in addition to the multipath interference considered in Section III, there is interference due to direct cross-pol to co-pol conversion, e.g., due to the cross-pol gain of the transmitting and receiving antennas. These components can be included in the general formulation developed in Section III. In Sections IV and V performance bounds are developed for the general multipath case

considered in Section III and conclusions are given in Section VI. An inherent assumption in the analyses presented in this article, is that the co-pol and cross-pol channels are quasi-static (relative to many symbol periods). Thus these analyses will not accurately model a fast-fading scenario.

II. Performance of OQPSK in the Presence of a Single Cross-Pol Interference

We assume that the interference OQPSK symbols, $I_n \equiv I_{xn} + jI_{yn}$, are independent from the desired OQPSK symbols, $S_n \equiv S_{xn} + jS_{yn}$, and in fact are generated from the S_n by an integer delay Δ , i.e., $I_n = S_{n-\Delta}$. The symbol boundaries of the desired OQPSK signal are aligned with the symbol boundaries of interference in this analysis. This represents the worst case interference in terms of the arrival time of the interference symbol boundaries. We analyze the case where the signal is contaminated by additive, rotated, and scaled interference plus noise: $X_n \equiv S_n + \alpha e^{j\phi} I_n + N_n$, where φ is the rotation angle; N_n denotes the additive noise and $\alpha \equiv 10^{-XPD/20}$ is the amplitude of the interference, which is equal to the reciprocal of the XPD.

In Figure 2, we show a timing diagram of the received signal and the interference signal. The receive symbol, $S_{xn,}$ is aligned in time with the symbol boundaries of I-component of the interference, I_{xn}, and is offset in time by a half of a symbol with the Q-component, I_{yn}. During the symbol period, in addition to the interference from the I-component of the interference, I_{xn}, the Q-component of two adjacent symbols I_{yn} and I_{yn+1} can interfere with the detection of $S_{xn.}$ Similar diagram and analysis can be performed if the symbol boundaries of S_{xn} are aligned with the symbol boundaries of the Q-component of the interference.

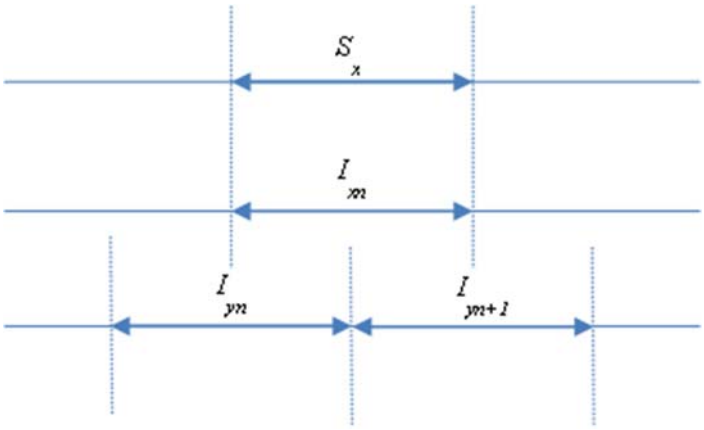

Figure 2. Timing diagram of received symbol S_{xn} and the I- and Q-components, I_{xn} and I_{yn}, of the interfering signal, $I_{n.}$.

In analyzing the uncoded OQPSK bit error rate (BER), we consider the following eight distinct cases:

Table 1. Eight distinct cases for uncoded OQPSK bit error rate.

I_{xn}	I_{yn}	I_{yn+1}	$(I_{yn}+I_{yn+1})/2$	$Real(e^{j\Phi}I_n)$	$Imag(e^{j\Phi}I_n)$
$+1/\sqrt{2}$	$+1/\sqrt{2}$	$-1/\sqrt{2}$	0	$\cos\varphi/\sqrt{2}$	$\sin\varphi/\sqrt{2}$
$+1/\sqrt{2}$	$+1/\sqrt{2}$	$+1/\sqrt{2}$	$+1/\sqrt{2}$	$(\cos\varphi-\sin\varphi)/\sqrt{2}$	$(\sin\varphi+\cos\varphi)/\sqrt{2}$
$+1/\sqrt{2}$	$-1/\sqrt{2}$	$+1/\sqrt{2}$	0	$\cos\varphi/\sqrt{2}$	$\sin\varphi/\sqrt{2}$
$+1/\sqrt{2}$	$-1/\sqrt{2}$	$-1/\sqrt{2}$	$-1/\sqrt{2}$	$(\cos\varphi+\sin\varphi)/\sqrt{2}$	$(\sin\varphi-\cos\varphi)/\sqrt{2}$
$-1/\sqrt{2}$	$+1/\sqrt{2}$	$-1/\sqrt{2}$	0	$-\cos\varphi/\sqrt{2}$	$-\sin\varphi/\sqrt{2}$
$-1/\sqrt{2}$	$+1/\sqrt{2}$	$+1/\sqrt{2}$	$+1/\sqrt{2}$	$(-\cos\varphi-\sin\varphi)/\sqrt{2}$	$(-\sin\varphi+\cos\varphi)/\sqrt{2}$
$-1/\sqrt{2}$	$-1/\sqrt{2}$	$+1/\sqrt{2}$	0	$-\cos\varphi/\sqrt{2}$	$-\sin\varphi/\sqrt{2}$
$-1/\sqrt{2}$	$-1/\sqrt{2}$	$-1/\sqrt{2}$	$-1/\sqrt{2}$	$(-\cos\varphi+\sin\varphi)/\sqrt{2}$	$(-\sin\varphi-\cos\varphi)/\sqrt{2}$

Table 1 reflects the fact that I_{yn} is a half symbol delay from I_{xn} and S_{xn}. Consequently, both half symbols, I_{yn} and I_{yn+1}, are indicated along with their average $(I_{yn}+I_{yn+1})/2$. To detect S_{xn}, we integrate across $\mathrm{Real}(X_n)$ in which case the contribution from I_{yn} and I_{yn+1} is their average in the fourth column of the table.

We now see that the detection of S_{xn} is either enhanced or degraded by the additive term: $\alpha \cdot Real(e^{j\Phi}I_n)$. In particular, assuming Gaussian additive noise we can express the error probability in the detection of S_{xn} as an average of the eight corresponding complementary error functions, $erfc(\cdot)$:

$$\begin{aligned} P_{errx}(\phi,\alpha,E_b/N_0) \equiv \frac{1}{8}[&0.5erfc(\{1+\alpha\cos\phi\}\cdot\sqrt{E_b/N_0}) + 0.5erfc(\{1+\alpha(\cos\phi-\sin\phi)\}\cdot\sqrt{E_b/N_0}) + 0.5erfc(\{1+\alpha\cos\phi\}\cdot\sqrt{E_b/N_0}) + \\ &0.5erfc(\{1+\alpha(\cos\phi+\sin\phi)\}\cdot\sqrt{E_b/N_0}) + 0.5erfc(\{1-\alpha\cos\phi\}\cdot\sqrt{E_b/N_0}) + 0.5erfc(\{1-\alpha(\cos\phi+\sin\phi)\}\cdot\sqrt{E_b/N_0}) + \\ &0.5erfc(\{1-\alpha\cos\phi\}\cdot\sqrt{E_b/N_0}) + 0.5erfc(\{1-\alpha(\cos\phi-\sin\phi)\}\cdot\sqrt{E_b/N_0})], \end{aligned} \quad (1)$$

where we denote the error in detecting the S_{xn} by P_{errx}. A comparable analysis reveals that the error in detecting S_{yn} (denoted by P_{erry}) is identical to P_{errx}. Thus, the total uncoded bit error probability is given by: $0.5\cdot(P_{errx}+P_{erry})=P_{errx}$. The angular rotation of interference, φ, which produces the worst performance, depends on the XPD and the bit error rates. In general, for a moderate XPD of 12 dB and higher and BER of 10^{-3}, either $\varphi=0$ or $\varphi=\pi/2$ produces the worst BER performance. For very low BER, $\varphi=\pi/4$ corresponds to the worst BER performance.

We now consider the performance of uncoded OQPSK in the presence of cross-pol interference. Figure 3 shows the bit error rate (BER) performance of an uncoded OQPSK link with cross-pol interference at an XPD of 15 dB. Both analyses and simulations have been performed for interference phase rotations varying from 0° to 360° in 5° increments. The results of the simulations match closely with the results of the analyses.

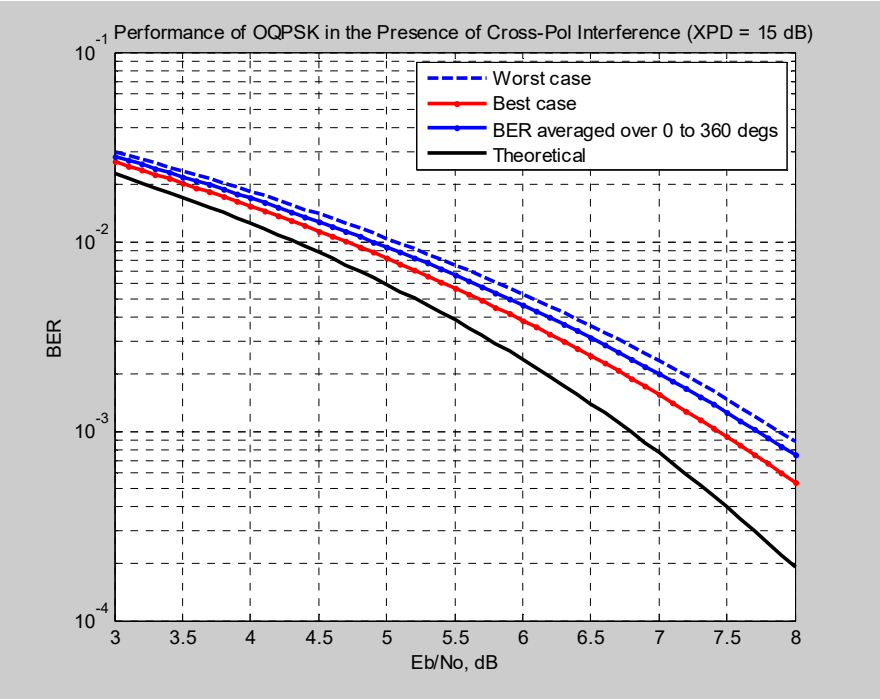

Figure 3. Performance of uncoded OQPSK in the presence of cross-pol interference with an XPD of 15 dB.

In Figure 3, the best case and the worst case OQPSK performance as a function of the interference phase rotation, φ , are shown as well as the theoretical performance of an OQPSK link without cross-pol interference. Figure 3 also shows the BER performance averaged over all interference phase rotations. For an uncoded BER of 10^{-3}, the worst case interference phase rotation degrades the link by approximately 1.1 dB compared to an OQPSK link without interference.[1]

Averaging over all interference phases, the cross-pol interference degrades the OQPSK link by 0.9 dB. Figure 4 shows the performance of an OQPSK link with a weaker cross-pol interference XPD of 25 dB. The figure shows the theoretical performance of an OQPSK link without interference and the best-case and worst-case performances of OQPSK with cross-pol interference as a function of the interference phase rotations. For BER of 10^{-3}, the worst-case interference phase rotation degrades the link by about 0.1 dB.

[1] The dual-polarization OQPSK X-band downlink for SWOT uses Reed-Solomon (255,223) code with an interleaving depth of five. The frame error rate (FER) requirement for SWOT is 1.3×10^{-7}. That corresponds to an uncoded Reed-Solomon input error rate of 1.5×10^{-3} and Reed-Solomon output bit error rate of 2.2×10^{-10}. For this article, uncoded BER of 10^{-3} is used as the SWOT operating threshold.

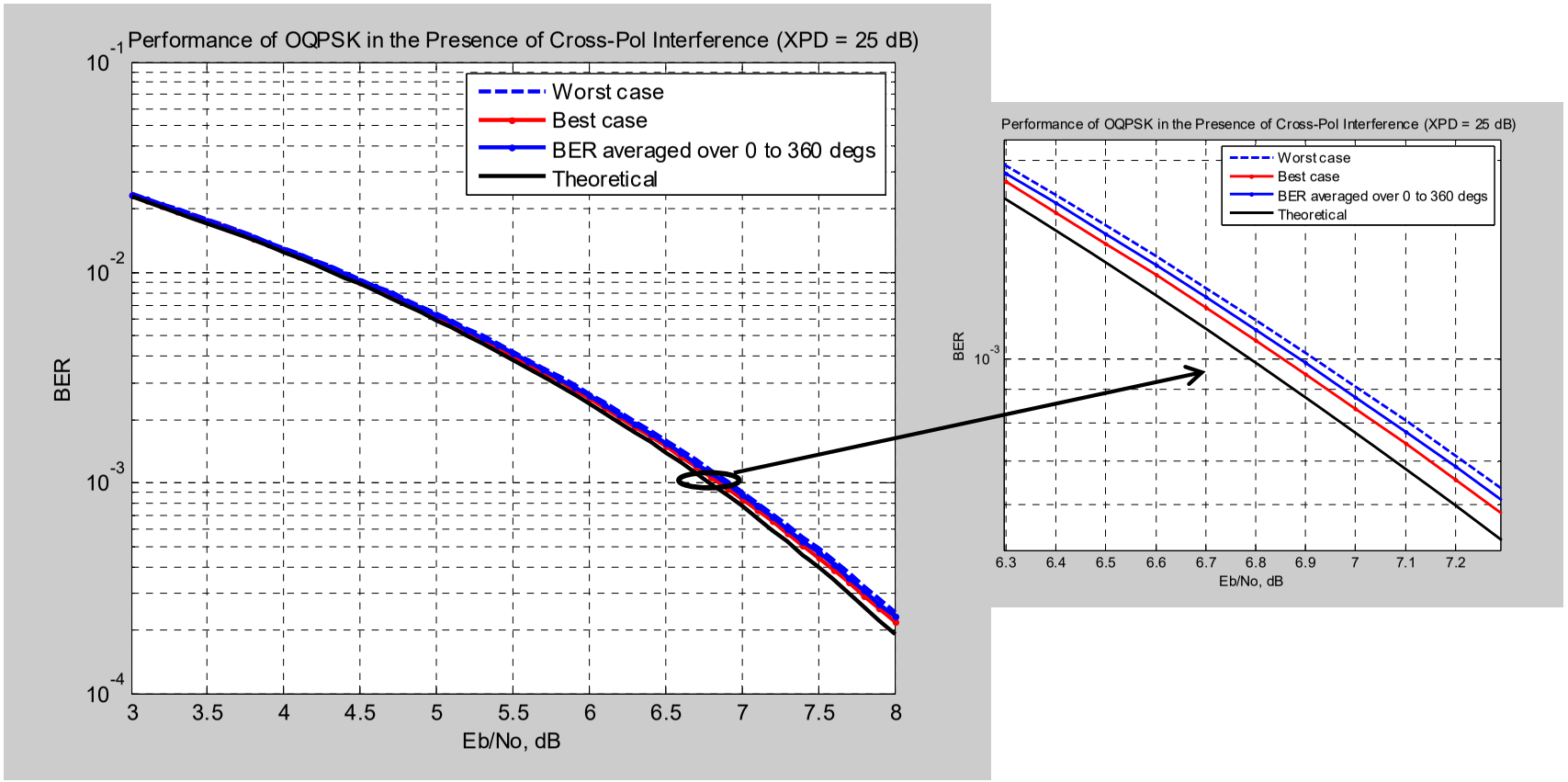

Figure 4. Performance of uncoded OQPSK in the presence of cross-pol interference with XPD of 25 dB.

Figure 5 shows the degradation to uncoded OQPSK links at BER of 10^{-3} for the worst case interference phase rotations over the XPD range of 10 dB to 25 dB. The figure also shows a degradation upper bound given by

$$\text{Degradation (dB)} \leq -20 \cdot log_{10}(1 - 10^{-XPD/20}). \quad (2)$$

The degradation computed using this bound is about 0.6 dB worse than obtained from the analysis for an XPD of 15 dB. Figure 5 shows that for an XPD of 15.5 dB and higher (blue curve), the degradation due to cross-pol interference is less than 1 dB. For an XPD of 19 dB and higher, the degradation is less than 0.5 dB.

We have also examined the impact of cross-pol interference on coded system performance. Specifically, simulations have been performed with and without interference using the (255,223) Reed-Solomon (RS) decoder. The results shown in Figure 6 correspond to an XPD of 15 dB. The solid curve for the no interference case is computed using the uncoded symbol error rate performance of QPSK/OQPSK at the input to the RS decoder. Figure 6 also shows the BER performance of the coded OQPSK links with cross-pol interference for the best case and the worst case interference phase rotations. These curves for OQPSK links are computed using the input symbol error rate formula derived in Equation (1).

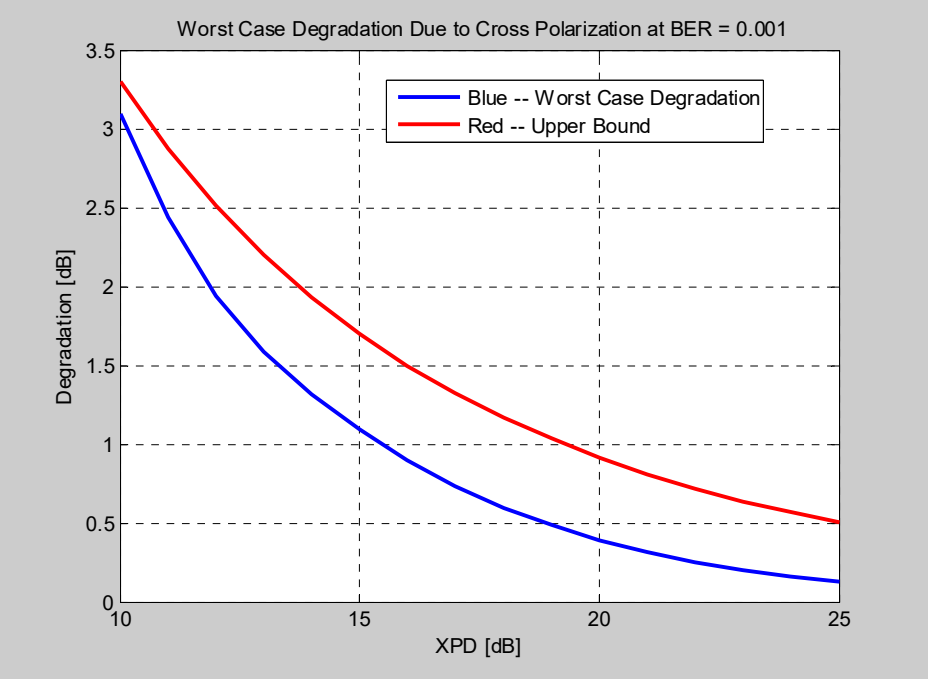

Figure 5. Worst-case degradations of OQPSK links in the presence of cross-pol interference with an XPD ranging from 10 dB to 25 dB for a BER of 10^{-3}.

As seen from Figure 6, the simulated RS performance of OQPSK matches closely with the computed BER performance with the RS code. Due to the computational constraints, simulations have only been performed for RS output BER down to approximately 10^{-6}. To estimate the loss due to cross-pol interference at the SWOT operational BER threshold of 2.2×10^{-10}, the solid curves based on the computed RS performance are used. It is seen that

for the worst case interference phase rotation, the cross-pol interference degrades the OQPSK link by 1.1 dB for a BER of 2.2 x 10^{-10}.

Figure 7 shows the computed RS performance in the presence of cross-pol interference with an XPD of 25 dB. For such weak cross-pol interference, the worst case interference phase rotation degrades the OQPSK link by only 0.2 dB.

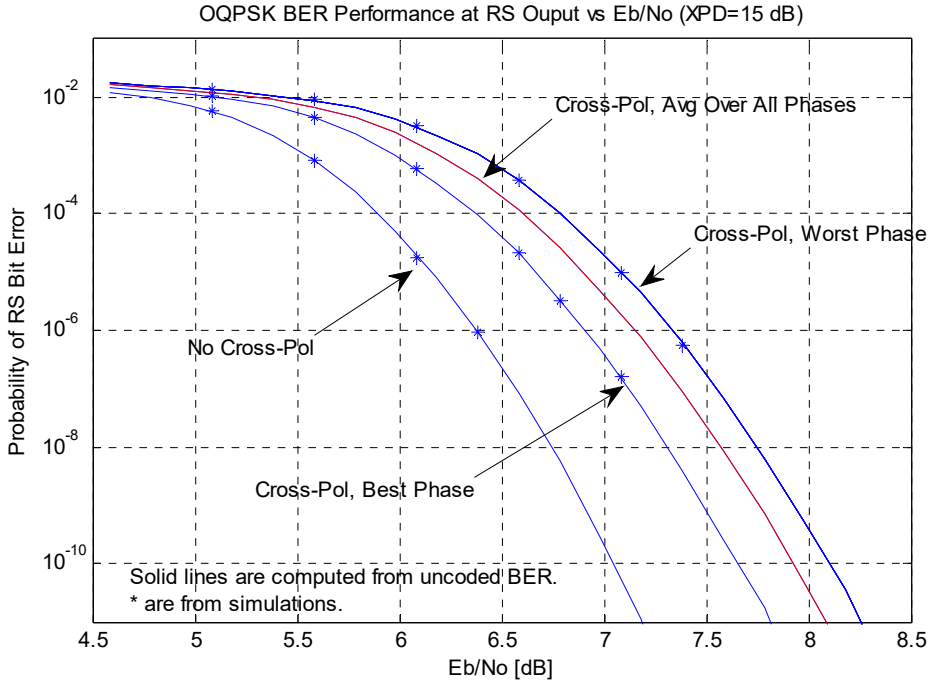

Figure 6. OQPSK BER performance at the output of Reed-Solomon decoder for XPD of 15 dB.

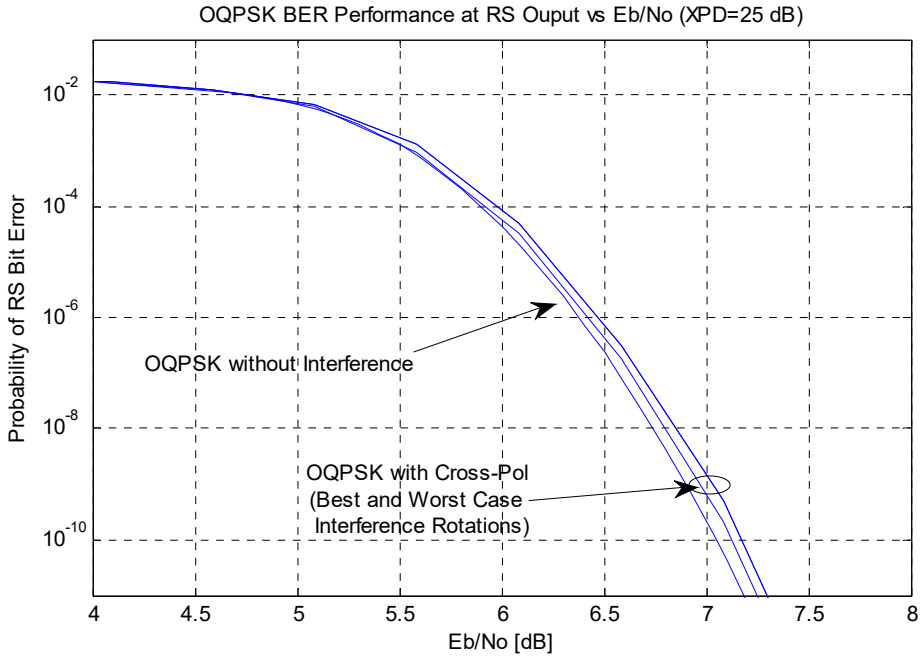

Figure 7. OQPSK BER performance at the output of Reed-Solomon decoder for XPD of 25 dB.

III. Performance of OQPSK in the Presence of Multiple Cross-Polarization Interference Components with Multipath

Here we assume that the multipath interference OQPSK symbols, $I_n \equiv I_{xn} + jI_{yn}$, are independent of the desired OQPSK symbols, $S_n \equiv S_{xn} + jS_{yn}$, and arise from spacecraft reflections of the cross-pol signal at which point they become co-pol interference. In the following, we analyze the scenario wherein the signal is contaminated by multiple (M) additive, rotated and delayed interferers plus noise:

$$X_n \equiv S_n + \sum_{k=1}^{M} A_k e^{j\phi_k} I_{n-\delta_k} + N_n \tag{3}$$

where A_k, φ_k, δ_k denote respectively the amplitude, phase rotation and delay of the k^{th} interference multipath component relative to S_n and N_n denotes the additive noise. Here we assume that: $A_k = 10^{-(XPD_k/20)}$ where XPD_k can be considered as the ratio of the power of the desired co-pol signal divided to the power of the k^{th} multipath interference. Therefore, XPD_k represents the cross-pol discrimination of the k^{th} path. Note that this analysis extends that presented in [2] to wideband signaling.

In Figure 8, we show a timing diagram of the received signal and a single (multipath) interference signal with delay δ relative to the desired signal. The receive symbol, $S_{xn,}$ is offset in time by δ from the symbol boundaries of the I-component of the interference, I_{xn}, and is offset in time by half of a symbol plus δ, i.e., $T_s/2+\delta$, with the Q-component, I_{yn}. (Here we assume that T_s is normalized to unity.) During the symbol period, in addition to the interference from the I-component of the interference, I_{xn}, the Q-component of two adjacent interference symbols, I_{yn} and I_{yn+1}, will also interfere with the detection of S_{xn} as well as the I-component of the adjacent symbol I_{xn-1}, assuming $0 \le \delta \le T_s/2$. If $T_s/2 \le \delta \le T_s$, then in addition to I_{yn}, I_{yn+1} and I_{xn-1} the Q-component of I_{yn-1} will also interfere with the detection of S_{xn}. This corresponds to a total of 5 interference symbols that can interfere with the detection of S_{xn}, i.e., $I_{yn-1,}$ I_{yn}, $I_{yn+1,}$ I_{xn} and I_{xn-1}. Assuming that each of these symbols are binary-valued (± 1), then a total of $2^5 = 32$ combinations of these interference symbols can interfere with the detection of S_{xn}. If $0 \le \delta \le 2T_s$, this expands to 7 interference symbols: $I_{yn-2,}$ $I_{yn-1,}$ I_{yn}, $I_{yn+1,}$ $I_{xn,}$ I_{xn-1} and I_{xn-2}, and thus 128, equally likely combinations. In the following, we will restrict attention to this range of δ as it corresponds to the delay spread typically associated with scattering from the spacecraft.

In analyzing the uncoded OQPSK BER, we consider the following distinct cases for the real part of the interference amplitude for the k^{th} multipath component:

$$A(A_k,\varphi_k,\delta_k) \equiv \begin{cases} A_k\left\{\cos\varphi_k \cdot \left(\delta_k I_{xn-1} + (1-\delta_k)\cdot I_{xn}\right) - \sin\varphi_k \cdot \left((0.5+\delta_k)I_{yn} + (0.5-\delta_k)\cdot I_{yn+1}\right)\right\}, 0 \le \delta_k \le 0.5 \\ A_k\left\{\cos\varphi_k \cdot \left(\delta_k I_{xn-1} + (1-\delta_k)\cdot I_{xn}\right) - \sin\varphi_k \cdot \left((1.5-\delta_k)I_{yn} + (\delta_k-0.5)\cdot I_{yn-1}\right)\right\}, 0.5 \le \delta_k \le 1 \\ A_k\left\{\cos\varphi_k \cdot \left((\delta_k-1)\cdot I_{xn-2} + (2-\delta_k)\cdot I_{xn-1}\right) - \sin\varphi_k \cdot \left((1.5-\delta_k)I_{yn} + (\delta_k-0.5)\cdot I_{yn-1}\right)\right\}, 1 \le \delta_k \le 1.5 \\ A_k\left\{\cos\varphi_k \cdot \left((\delta_k-1)\cdot I_{xn-2} + (2-\delta_k)\cdot I_{xn-1}\right) - \sin\varphi_k \cdot \left((2.5-\delta_k)I_{yn-1} + (\delta_k-1.5)\cdot I_{yn-2}\right)\right\}, 1.5 \le \delta_k \le 2 \end{cases} \tag{4}$$

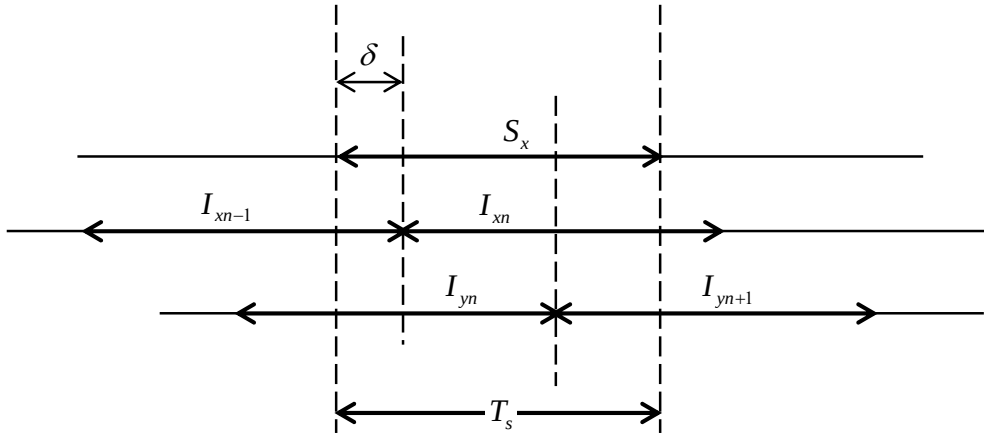

Figure 8. Timing diagram of received symbol S_{xn} and the I- and Q-components, I_{xn} and I_{yn}, of a single interfering signal, I_n.

From Equation (4), we can see that the detection of S_{xn} is either enhanced or degraded by the additive term $\text{Real}(e^{j\phi}I_n)$. In particular, assuming Gaussian additive noise we can express the error probability in the detection of S_{xn} as an average of the 128 corresponding complementary error functions, $erfc(\cdot)$.[2]

$$P_{err}(E_b/N_0) \equiv \frac{1}{128}\cdot\left\{\sum_{(I_{xn-2}=\pm1, I_{xn-1}=\pm1, I_{xn}=\pm1, I_{yn-2}=\pm1, I_{yn-1}=\pm1, I_{yn}=\pm1, I_{yn+1}=\pm1)} 0.5\cdot erfc\left(\left[1+\sum_{k=1}^{M} A(A_k,\varphi_k,\delta_k)\right]\cdot\sqrt{E_b/N_0}\right)\right\}. \quad (5)$$

In Equation (5) it is assumed that $S_{xn}=+1$ which is sufficient as the opposite polarity is redundant. The composite XPD is the reciprocal of the combined interference power and is defined by:

$$\langle XPD\rangle \equiv 1/P_I = 1/\left|\sum_{k=1}^{M} A_k\cdot e^{j\varphi_k}\right|^2 \quad (6)$$

P_I is the power that is computed by the antenna model [3], [4] that is used to predict SWOT performance. The model is a narrowband model based on an unmodulated continuous wave (CW) transmission. Note that P_I is always less than the perfectly coherent limit, i.e.,

$$0 \le P_I \le \left|\sum_{k=1}^{M} A_k\right|^2 \quad (7)$$

$\langle XPD\rangle$ is typically the only observable generated by the predictive antenna model that is related to the composite cross-pol interference.

Figure 9 shows the bit error rate (BER) performance of an uncoded OQPSK link with $M = 3$ cross-pol multipath interference components at $XPD_1 = 21.2$ dB and $XPD_2 = XPD_3 = 20$ dB.

---

[2] We note that E_b/N_0 in Equation (5) corresponds to a single rail, i.e., in-phase or quadrature channel. Due to symmetry the BER is the same in each rail.

Both analyses in Equation (5) and in simulations have been compared for interference multipath delays of $\delta_1 = 2/16$, $\delta_2 = 12/16$, and $\delta_3 = 15/16$ relative to the desired signal. These delays in turn create phase rotations φ_k given by, $\varphi_k = -2\pi(\delta_k / R_s) \cdot f_0$, where R_s denotes the symbol rate[3] and f_0 denotes the X-band carrier frequency (assumed to be 8.2 GHz). With these parameters, the corresponding carrier phase rotations for the three interference multipath components (modulo 360 deg) are $\varphi_1 = 139.3$ deg, $\varphi_2 = 116.1$ deg, and $\varphi_3 = 145.1$ deg. In addition, a random phase rotation $\delta\varphi$ was added to these phase rotations, i.e., $\varphi_k \leftarrow \varphi_k + \delta\varphi$. The composite $\langle XPD \rangle$ for this case is about 11.1 dB. The results of the simulations match closely with the results of the multipath analysis.

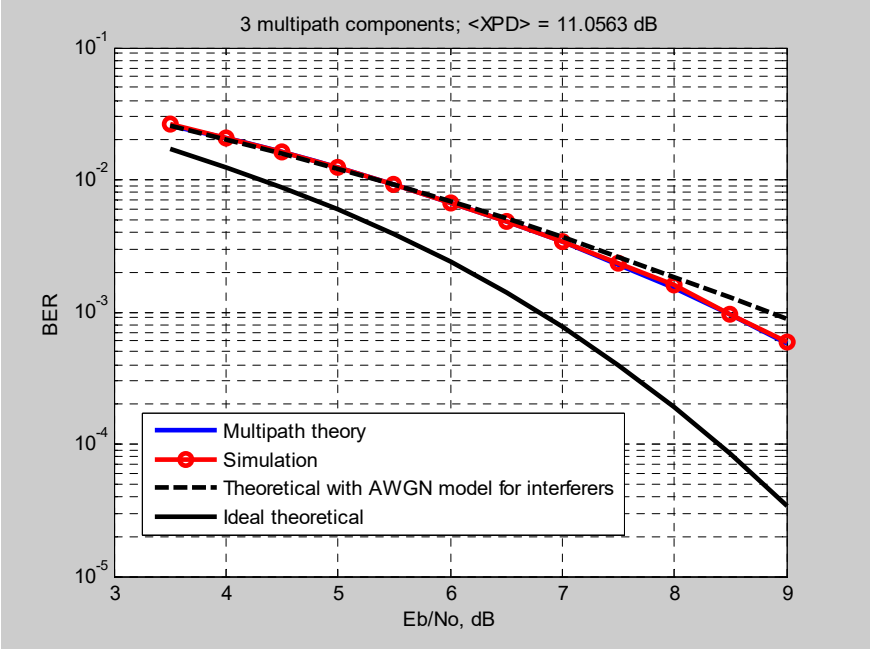

Figure 9. Performance of uncoded OQPSK in the presence of multipath cross-pol interference: comparable XPDs.

Also shown in Figure 9 is a curve based on an analysis that models the sum of the three interferer multipaths as an additive white Gaussian noise (AWGN) component with total power = $\langle XPD \rangle$. This curve is computed from:

$$P_{err}^{AWGN}(E_b / N_0) \equiv 0.5 \cdot erfc\left(\sqrt{\overline{E_b / N_0}}\right), \tag{8a}$$

where $\overline{E_b / N_0}$ denotes the effective E_b / N_0 and is given by:

$$\overline{E_b / N_0} = \frac{1}{(E_b / N_0)^{-1} + <XPD>^{-1}}, \tag{8b}$$

and $<XPD>$ is obtained from Equation (6). Note that as E_b / N_0 increases, $\overline{E_b / N_0}$ approaches $<XPD>$, thereby creating an error floor in P_{err}^{AWGN}. As is seen, in this case the AWGN curve is in close agreement with the multipath theory curve except for a slight overestimate above E_b / N_0 = 8 dB. The difference between the curves depends on P_I, which is bounded as indicated in Equation (7). Note also that for an uncoded BER of 10^{-3},

[3] In the remainder of this article and without loss of generality, it is assumed that R_s = 155 Msps, i.e., the symbol rate prior to Reed-Solomon encoding.

the multipath interference degrades the link by approximately 1.7 dB compared to an OQPSK link without interference (ideal theoretical curve in Figure 9).

Figure 10 shows the BER performance of an uncoded OQPSK link with P = 3 cross-pol multipath interference components but with amplitudes at $XPD_1 = 21.2$ dB, $XPD_2 = 15$ dB, and $XPD_3 = 12$ dB and with interference multipath delays of $\delta_1 = 0$, $\delta_2 = 11/16$, and $\delta_3 = 6/16$ relative to the desired signal. In addition, the curve corresponding to the AWGN interferer model is shown. For this case, the multipath theory curve correctly models the simulation curve and we see that the AWGN model underestimates the multipath theory curve. Note also that for an uncoded BER of 10^{-3}, the multipath interference degrades the link by approximately 1.2 dB compared to an OQPSK link without interference.

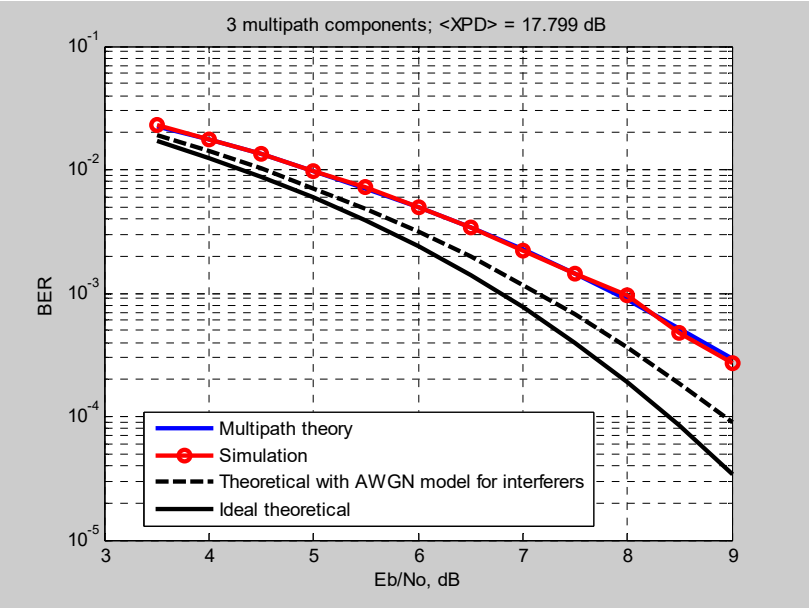

Figure 10. Performance of uncoded OQPSK in the presence of three multipath cross-pol interferers with disparate XPDs.

Figure 11 shows the BER performance of an uncoded OQPSK link again with P = 9 cross-pol multipath interference components but with amplitudes at $XPD_1 = 21.2$ dB, $XPD_2 = 20$ dB= $XPD_3 = \ldots = XPD_9$ and with interference multipath delays of, $\delta_1 = 5/16$, $\delta_2 = 12/16$, $\delta_3 = 8/16$, $\delta_4 = 14/16$, $\delta_5 = 6/16$, $\delta_6 = 12/16$, $\delta_7 = 8/16$, $\delta_8 = 13/16$, and $\delta_9 = 0$ relative to the desired signal (the two redundant delays in this example, 8/16 and 12/16, were purely coincidental). In addition, the curve corresponding to the AWGN interferer model is shown which in this case agrees quite closely with the multipath theory curve and simulation. Note also that for an uncoded BER of 10^{-3}, the multipath interference degrades the link by approximately 1 dB compared to an OQPSK link without interference.

Note from Figures 9–11 that the AWGN model either closely approximates the multipath theory model or underestimates it as in the cases of Figures 10–11. The difference depends on P_I which is bounded as indicated in Equation (7). Specifically, for small P_I the AWGN model underestimates the exact BER curve and vice versa for a larger P_I, e.g., Figure 9 at

E_b / N_0 > 8 dB. Clearly the AWGN model cannot be used to provide a consistent worst-case system performance bound. Developing a worst case bound is discussed further in the next section.

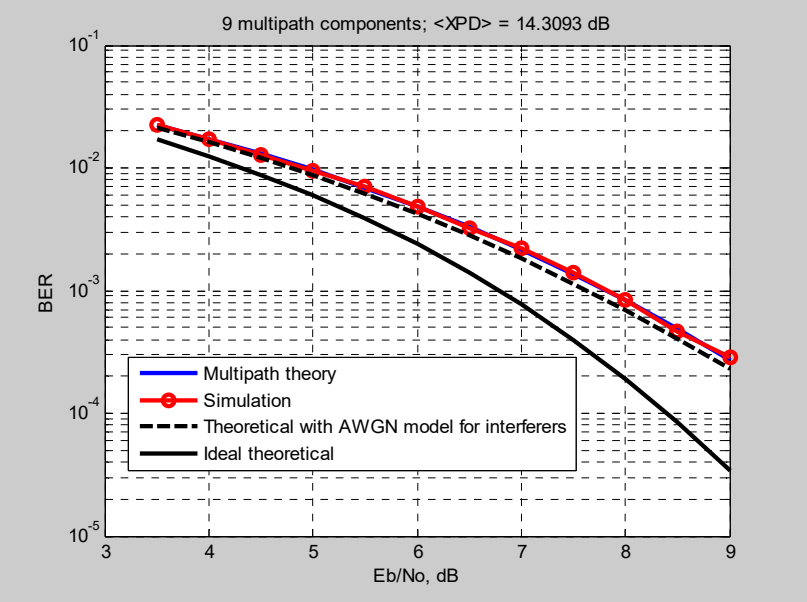

Figure 11. Performance of an uncoded OQPSK in the presence of nine multipath cross-pol interference components.

IV. Bounding System Performance using a Single Cross-pol Interferer Model

As noted in Section III, the antenna model [3], [4] that is used to predict SWOT performance is a narrowband model based on an unmodulated CW transmission and the effective XPD, as in Equation (6), is typically the only observable parameter generated by the predictive antenna model. Given that the exact theoretical multipath model depends on multiple parameters {phase, amplitude, and delay of each multipath signal component—see Equation (5)}—not provided by the predictive model; it is of limited practical utility in predicting system performance. Consequently, we consider here a simpler single-user OQPSK model, dependent only on a single, effective XPD, to provide a worst case bound on system performance (for purposes of link budget planning).

In Section II, the impact of a single co-channel interferer on system performance was analyzed. There it was assumed that the interferer was synchronous with the desired signal (zero relative delay) but was offset in phase.[4] Interestingly, it turns out this analysis is useful in bounding performance for more realistic scenarios. In the absence of weather effects, there are several sources of cross-pol interference: (i) cross-pol transmit signal that is converted to a co-pol signal by the cross-pol gain of the receiving antenna; (ii) cross-pol transmit signal that is converted to a co-pol signal by the cross-pol gain of the transmitting antenna; and received through the receiving antenna's co-pol gain and (iii) reflections of

[4] Note that this is a special case of Equation (5).

the cross-pol transmit signal off the surrounding spacecraft structures and received through the receiving antenna's co-pol gain (as analyzed above). The situation is further complicated by the presence of weather effects that can also convert the signal polarization from cross- to co-pol and vice versa.

Initially ignoring reflections, we assume that all cross- to co-pol conversions affect only amplitude and not phase. In such cases, the cross-pol interference sources all add together in phase producing a large, effective XPD. Specifically, based on current estimates of the various cross-pol to co-pol conversion amplitudes (SWOT receive/transmit antennas as well as weather effects), we have that typical cross to co-pol conversion amplitudes, based on the SWOT antennas, are: –23.4 dB (transmit antenna);[5] –24.8 dB (receive antenna); and –23.5 dB (weather). The –23.4 dB contribution for the transmit antenna is from coupling due to cross-pol gain of the transmit antenna in free-space. This does not include the contributions of multipath due to reflections off the spacecraft. Assuming these components add together in phase, the combined cross-pol generated interference amplitude corresponds to an effective XPD of 14.3 dB. Of course, this is the worst case based on the assumption that all cross- to co-pol conversions affect only amplitude and not phase. In general, we would expect the effective XPD to be larger than this.

We now consider the effects of the reflections of the cross-pol transmit signal off the surrounding spacecraft structures (i.e., cross-pol multipath). Based on the antenna model that has been developed to predict SWOT performance, we find that taking into account the reflections of the transmitted cross-pol signal the effective XPD varies by about +/- 4 dB around the –23.4 dB cross-pol signal that is converted to co-pol by the transmit antenna. Based on computer simulations of 10,000 realizations of multipath reflections, we find that this variation can be achieved for two reflected paths with delay spreads ranging from 0 to 1 symbol period and amplitude spreads of 4 dB about a mean amplitude level of –37.4 dB.

For each realization, we randomly selected the path delays as well as the amplitudes of the reflected paths. Combining these reflected paths together with the above transmit/receive/weather cross-pol interference (again assuming a worst-case combined amplitude of –14.3 dB), we have generated the distribution of the total effective XPD (over 300 randomly selected realizations out of the 10,000 generated) as shown in Figure 12. Note that even though the reflected components are about 23 dB lower than the direct (–14.3 dB) component, there is still substantial (~ $\pm$1.5 dB) fluctuation in the total XPD.

Given this model, we compared the single-user model (using the worst-case BER over all rotations between 0 and 90 deg) with the exact multipath BER model from Equation (5). Specifically, for each realization we compute the difference in E_b / N_0 at 10^{-3} BER between the single-user, worst-case BER and the exact BER. The resulting histogram of this E_b / N_0 difference over all 10,000 realizations is shown in Figure 13. As is seen, the single-user model provides a very good upper bound on system performance (overestimating performance in only 0.5 percent of the 10,000 realizations generated).

[5] Based on the antenna model that has been developed to predict SWOT performance ([3], [4]).

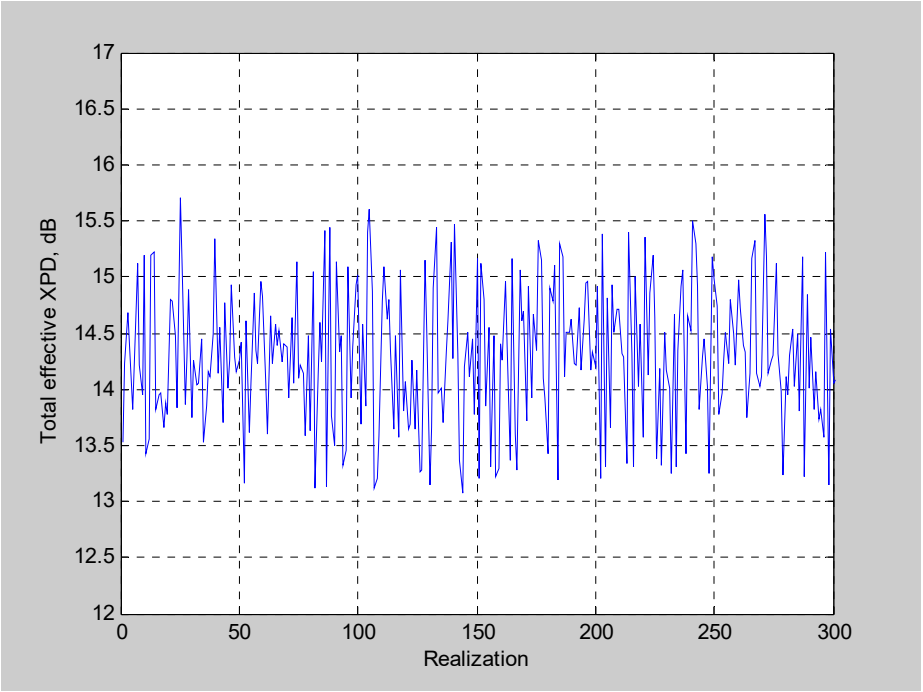

Figure 12. Sample distribution of total effective XPD with direct and reflected paths.

As an alternate (simpler) bound on system performance for this case, we again utilize the single-user model but with a zero degree rotation and an overall amplitude of about 0.6 dB larger than the direct (–14.3 dB) component. This accounts for amplitude fluctuations induced by the multipath components[6]. The resulting histogram is shown in Figure 14. As is seen, this bound provides a slightly more pessimistic estimate of system performance (by about 0.2 dB), but overall it is quite good and is simpler to compute.

[6] Specifically, 0.6 dB is the difference between the composite XPD including the two modeled reflected paths as described above and the composite XPD excluding the reflected paths.

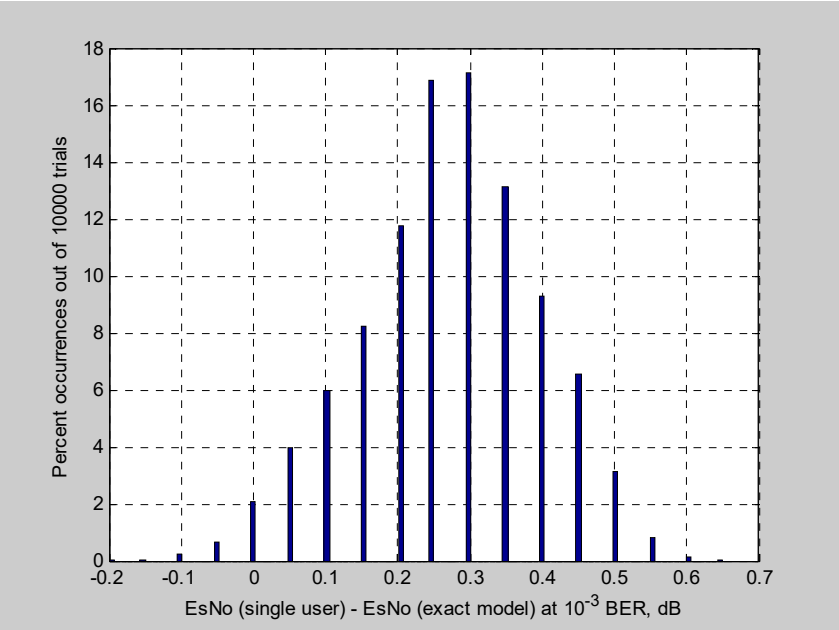

Figure 13. Sample distribution of the difference in E_b / N_0 at 10^{-3} BER.

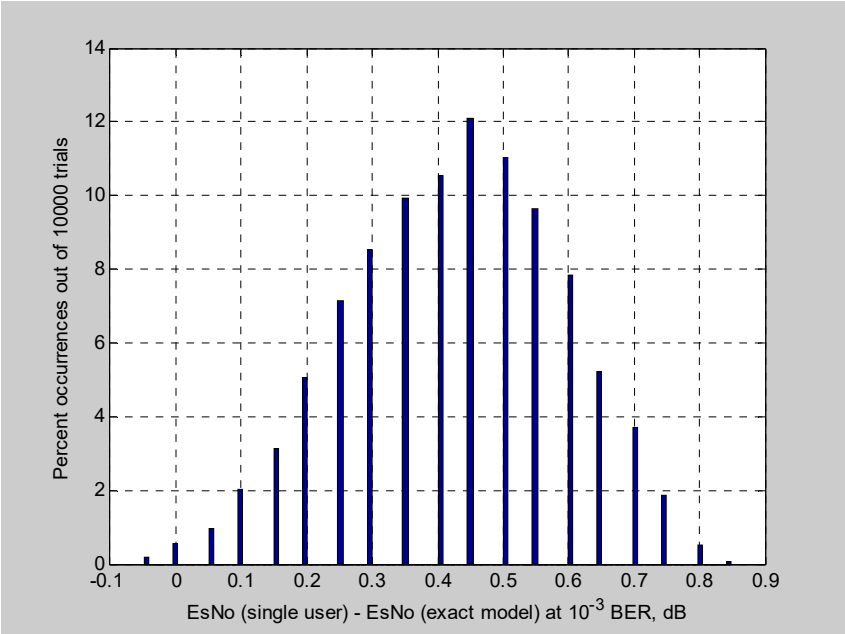

Figure 14. Sample distribution of the difference in E_b / N_0 at 10^{-3} BER assuming a worst case XPD of 13.7 dB.

V. Bounding System Performance using Cross-pol Interferer Frequency Selectivity

Here we consider a different single-user OQPSK model, dependent only on a single, effective XPD, to provide a worst case bound on system performance. This bound is related to the frequency selectivity of the cross-pol multipath. Specifically, when observing the spectrum of the cross-pol interference in multipath, $P_{Xpol}(f)$, we have the following model based on Equation (3):

$$P_{Xpol}(f) = P_I(f) \cdot \left|\sum_{k=1}^{M} A_k e^{j\phi_k}\, e^{-2\pi j \delta_k T_{sym} \cdot f}\right|^2 \equiv P_I(f) \cdot |H_{chan}(f)|^2, \tag{9}$$

where $P_I(f)$ denotes the spectrum of the cross-pol interference as a function of frequency (Hz), A_k, ϕ_k are as defined in Equation (3), T_{sym} is the symbol interval in seconds, and ($\delta_k T_{sym}$ is the delay in seconds of the kth multipath. Plots of $|H_{chan}(f)|^2$ (dB) (including the matched filter response) are shown in Figure 15 corresponding to the parameters used in Figures 9 and 10.

These plots further reinforce the BER results shown in Figures 9 and 10. In particular, we see from Figure 15A that the cross-pol interference channel response peaks at around –11 dB centered within the signal passband corresponding to the 1.7 dB degradation at 10^{-3} BER as previously noted. However, as seen from Figure 15B, the cross-pol interference channel response is actually smallest (–18 dB) at the center of the signal passband. It does peak outside the signal passband but this is where the symbol matched filter response would attenuate the interference spectrum (as well as the interference spectrum $P_I(f)$ itself). Consequently, the 10^{-3} BER degradation is smaller (~ 1.2 dB as noted previously).

These examples suggest that an upper bound on system performance can be obtained by replacing the frequency-selective multipath channel with a flat fading model comprising a direct path interferer with XPD (dB) set to minus the maximum of the multipath channel response, i.e.,

$$XPD = -\max_{|f \cdot T_{sym}| \le 1} \{10 \cdot log_{10}(|H_{chan}(f)|^2)\} \tag{10}$$

For example, in the case of Figure 15A, we would bound system performance with a single interferer at approximately 11 dB XPD. In the case of Figure 15B, we would bound system performance with a single interferer at approximately 7 dB XPD (noting from Equation (10) that we use the maximum of the multipath channel response over the signal band, $|f \cdot T_{sym}| \le 1$). However, we use instead 12 dB XPD corresponding to the multipath channel response at the lower band edge in Figure 15B, i.e., at $f \cdot T_{sym} = -1$. The corresponding BER plots, including the flat fading, single interferer bound, are shown in Figure 16.

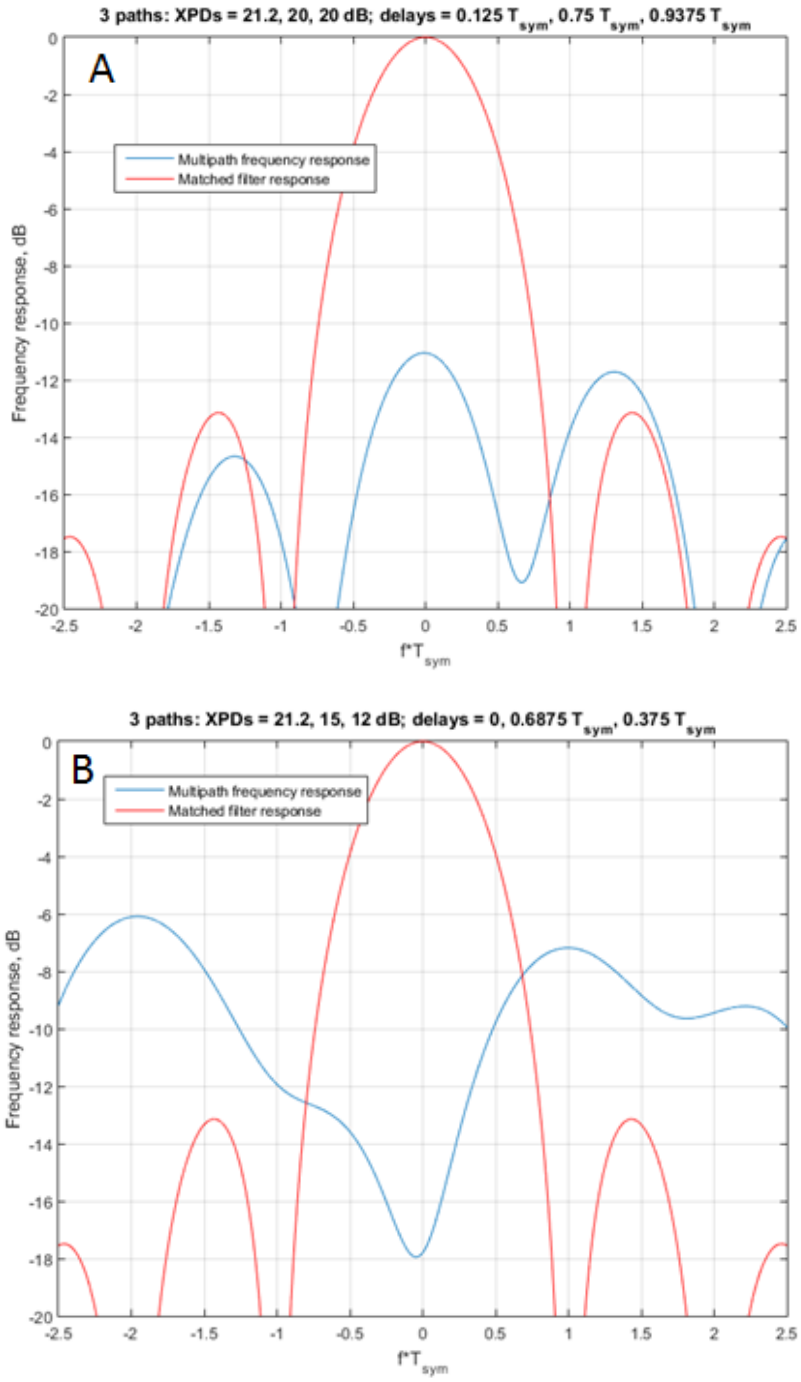

Figure 15. Frequency selectivity of multipath channels. (A) Multipath parameters corresponding to Figure 9. (B) Multipath parameters corresponding to Figure 10.

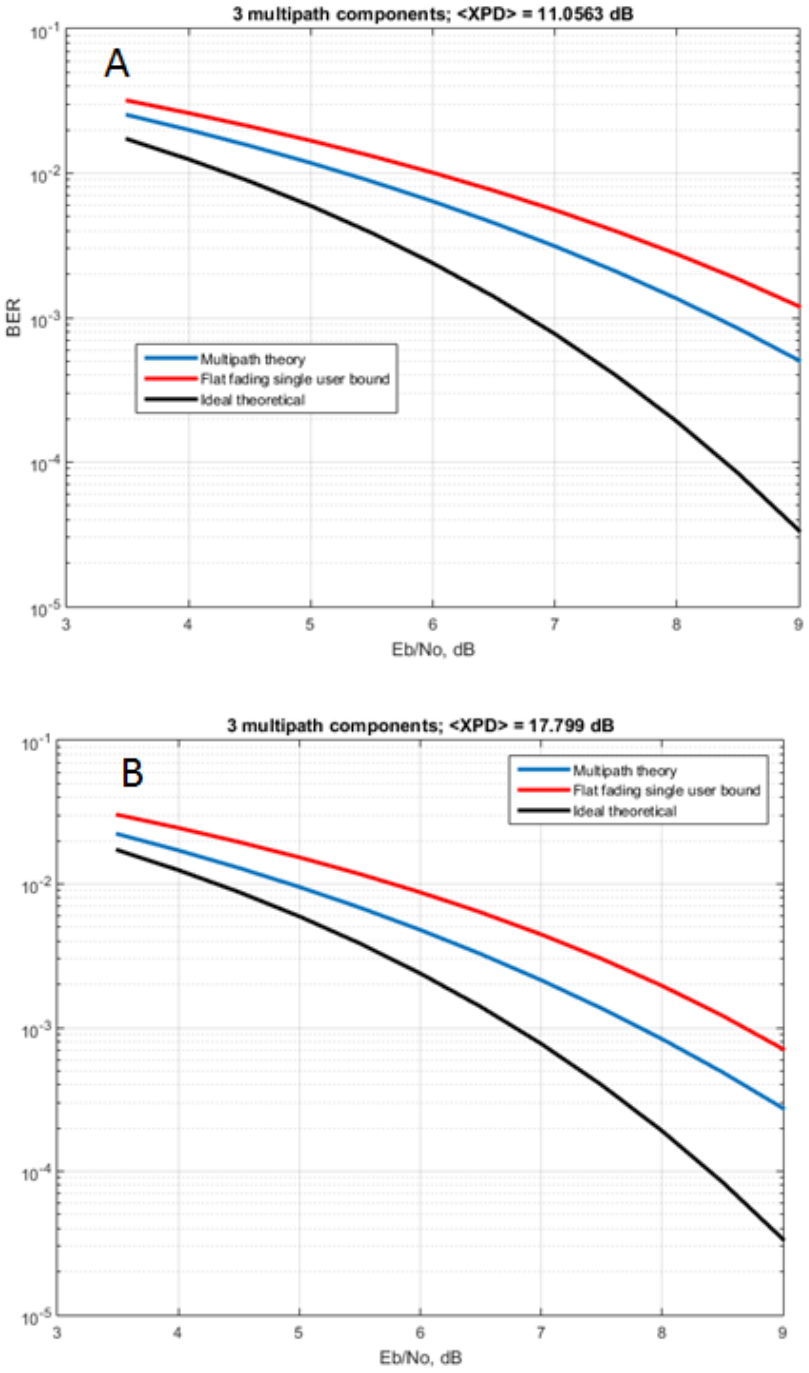

Figure 16. BER of multipath channels. (A) Multipath parameters corresponding to Figure 9. (B) Multipath parameters corresponding to Figure 10.

As seen, in both cases the bound is about 1 dB worse at 10^{-3} BER than the predicted performance (from multipath theory). We note in the case of Figure 15B that had we used the upper XPD bound from Equation (10), i.e., 7 dB, then the flat fading single co-pol user bound would have been much worse than that shown in Figure 16B. Clearly, the single co-pol user XPD bound from Equation (10) provides a worst case bound on system

performance; however, we can produce a tighter upper bound by replacing Equation (10) with:[7]

$$XPD = -\max_{|f \cdot T_{sym}| \le 1} \{10 \cdot log_{10}(|H_{chan}(f)|^2 \cdot |H_{match}(f)|^2)\}, \tag{11a}$$

where $|H_{match}(f)|^2$ denotes the magnitude-squared match filter response:

$$|H_{match}(f)|^2 = \left|\frac{\sin(\pi f T_{sym})}{\pi f T_{sym}}\right|^2 \tag{11b}$$

In this way, the channel response is weighted by the matched filter response, which deemphasizes peaks in $|H_{match}(f)|^2$ where the match filter response is small, i.e., near the band edges. With reference to Figure 15A, it is seen that the XPD bound from either Equation (10) or (11) will be about the same since $|H_{match}(f)|^2 \approx 1$ at the maximum of $|H_{chan}(f)|^2$. However in the case of Figure 15B, the XPD bound from Equation (11) is about 6.3 dB larger than that from (10) thereby producing a much tighter upper bound on system performance. A comparison of the two performance bounds for this channel is presented in Figure 17.

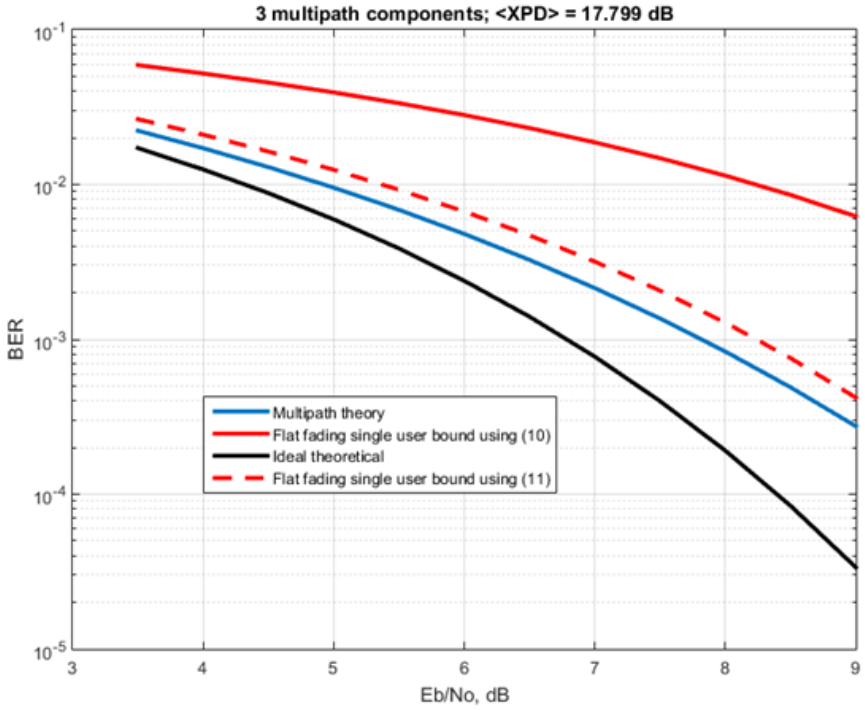

Figure 17. BER for multipath channel corresponding to Figure 15B comparing XPD bounds from Equations (10) and (11).

As can be seen, the XPD bound from Equation (11) results in a tighter upper performance bound than even shown in Figure 16B where the XPD bound from the lower band edge in Figure 15B was used. Specifically, the 10^{-3} BER degradation with the XPD bound from Equation (11) is only approximately 0.4 dB worse as seen in Figure 17.

[7] An even better approximation to system performance (not necessarily a bound) may potentially be obtained by replacing the max in Equation (11a) with the mean. However, this was not investigated in this study.

VI. Conclusion

Simulations and analyses have been performed for OQPSK in the presence of cross-pol interference: both a single interferer (Section II) and multiple multipath interferers (Section III). To meet the FER requirement of SWOT, it was shown in Section II that a single cross-pol interferer can cause up to 1.1 dB of degradation for XPD of 15 dB and 0.1 dB of degradation for XPD of 25 dB. Due to computational complexity of the Reed-Solomon decoder and the very low BER requirement for SWOT, simulations were not possible to estimate the degradation due to cross-pol interference for BER of 2.2×10^{-10} at the output of the Reed-Solomon decoder. Hardware testing will be needed to provide a more accurate estimate of the loss.

In Section III, we have developed a theoretical model for computing the performance of a dual polarization OQPSK link in the presence of multipath interference created by reflections of the cross-pol signal (transmitted from the cross-pol antenna). The theoretical model incorporates the time delays of the multipath components and is found to closely match simulation results. As a simpler approximation to the exact model, we have also considered an AWGN model, but we found that this can lead to an overestimation of system performance, and furthermore it predicts a fictitious error floor.

However, the theoretical model is limited in its application as it requires knowledge of the phase, amplitude and delay of each multipath signal component. These parameters are not available from the multipath statistics generated by the SWOT antenna model [3], [4] which only computes the composite XPD from Equation (6). This includes the cross-pol signal and its reflections from the spacecraft structure (multipath). However, the antenna model is narrowband and does not incorporate the OQPSK signal structure or the multipath delays associated with the spacecraft reflections. To this end we have also considered in Sections IV and V simple bounds on system performance, which can be computed based on data from the SWOT antenna model as well as spectrum analysis of the received co-pol interference signal. Overall these bounds are quite good and are simpler to compute.

The results presented in this article do not include the effects of transmit filtering, rain-induced attenuation, depolarization [5] and various other demodulation losses. It has been observed in simulations that symbol tracking loop errors at XPD of 10 dB can contribute significant losses for XPD of 10 dB and less. The losses due to these factors need to be taken into account to evaluate the end-to-end performance of the links.

References

[1] H. Vasseur, “Degradation of Availability Performance in Dual-Polarized Satellite Communications Systems,” *IEEE Transactions on Communications*, vol. 48, pp. 465–472, March 2000.

[2] V. K. Prabhu, “Error Rate Considerations for Coherent Phase-Shift Keyed Systems with Co-Channel Interference,” *The Bell System Technical Journal*, pp. 743–767, March 1969.

[3] N. Chahat, L. Amaro, J. Harrell, C. Wang, P. Estabrook, S. Butman, "X-Band Choke Ring Horn Telecom Antenna for Interference Mitigation on NASA's SWOT Mission," *IEEE Transactions on Antenna Propagation*, vol. 64, pp. 2075–2082, June 2016.

[4] H. H. Viskum, "CHAMP—The Dedicated Design Tool for Rotationally Symmetric Horns and Reflector Terminals," 2013 IEEE Antennas and Propagation Society International Symposium (APSURSI), pp. 2325–2326, July 2013.

[5] R. E. Castel and C. W. Bostian, "Combining the Effects of Rain-Induced Attenuation and Depolarization in Digital Satellite Systems," *IEEE Transactions on Aerospace and Electronic Systems*, vol. 15, pp. 299–300, March 1979.

Acronyms

AWGN	additive white Gaussian noise
BER	bit error rate
CNES	Centre National d'Etudes Spatiales (French space agency)
CW	continuous wave
co-pol	co-polarization
cross-pol	cross-polarization
deg	degree
ECH	externally corrugated horn
EGSE	electrical ground support equipment
EPC	electronic power conditioner
EESS	Earth Exploration Satellite Service
FER	frame error rate
GHz	gigahertz
Hz	hertz
LGA	low-gain antenna
LHCP	left hand circular polarization
Mbps	megabits per second
MHz	megahertz
Msps	megasymbols per second
OQPSK	offset quadrature phase-shift keying
RHCP	right hand circular polarization

RS	Reed-Solomon
SSR	solid state recorder
SWOT	Surface Water and Ocean Topography
TWT	traveling wave tube
TWTA	traveling wave tube amplifier
X-band	8–12 GHz
XPD	cross-polarization discrimination